Hindawi

Research Article

Photocatalytic and Biological Activities of Spherical Shape Cellulose/Silver Nanocomposites Using *Xenostegia tridentata* (L.) Leaf Extract

Shanmugam Chinnadurai ⓘ,[1] **Sathishkumar Saravanan** ⓘ,[1] **Sridevi Chinnathambi,**[1] **Sivakumar Sivalingam,**[1] **Govindhan Poongavanam,**[1] **Sivasubramanian Ganarajan,**[2] **Baskaran Krishnan,**[3] **Parthasarathi Bera,**[4] **Parameswaran Veembil Ramachandra Iyer,**[5] **and Liviu Mitu** ⓘ[6]

[1]*Advanced Biomaterial Laboratory, PG and Research Department of Chemistry, Sri Vijay Vidyalaya College of Arts and Science, Dharmapuri, Tamil Nadu 636807, India*
[2]*Advanced Multifunctional Materials and Analysis Laboratory (AMMAL), Department of Sciences, Amrita School of Physical Sciences, Amrita Vishwa Vidyapeetham, Coimbatore, Tamil Nadu 641112, India*
[3]*Department of Biochemistry, Sree Narayana Guru College, Coimbatore, Tamil Nadu 641105, India*
[4]*Surface Engineering Division, CSIR, National Aerospace Laboratories, Bangalore, India*
[5]*Department of Chemistry, Annamalai University, Annamalainagar, Chidambaram, Tamil Nadu, India*
[6]*Department of Physics & Chemistry, University of Pitesti, Pitesti 110040, Romania*

Correspondence should be addressed to Shanmugam Chinnadurai; chshanch@gmail.com, Sathishkumar Saravanan; sathish.sskg@gmail.com, and Liviu Mitu; ktm7ro@yahoo.com

A novel green synthesis of cellulose/Ag nanocomposites (Cell/XTLL Ag NCs) with in situ generated silver nanoparticles using *Xenostegia tridentata (L.)* leaf extracts (XTLL). The synthesized nanocomposites have been appreciably characterized by SEM, TEM, FT-IR, XRD, UV-Vis spectrometer, AFM, DRS, XPS, TGA, and ICP-OES. The Ag nanoparticles found for the Cell/XTLL 60 mM $AgNO_3$ have an average particle size of 33.78 nm. Moreover, Cell/XTLL Ag NC film, prepared with 60 mM $AgNO_3$, suggests greater antioxidant activity. The most potent cell/XTLL 60 mM $AgNO_3$ against *Escherichia coli*, *Staphylococcus aureus*, *Trichoderma viride,* and *Fusarium oxysporum* has strong antimicrobial activity and the best antimicrobial properties due to the fact that because the concentration of $AgNO_3$ solution increased, the zone of inhibition additionally accelerated. The Cell/XTLL 60 mM becomes examined in vitro for its ability of human tumor cell growth inhibitory impact on human breast cancer cell line MCF-7 using MTT assay. The catalytic activity of Cell/XTLL 60 mM $AgNO_3$ was assessed by the photocatalytic degradation of methylene blue and compared with bare cellulose. The Ag NPs are homogeneously unfolded out in Cell/XTLL 60 mM $AgNO_3$ which leads to low electron-hole recombination and accelerated dye adsorption. In particular, 100 mg of Cell/XTLL 60 mM $AgNO_3$, as catalyst, showed excellent photocatalytic activity with the efficiency of 91% degradation of methylene blue (MB).

1. Introduction

Silvernanoparticles with electrochemical, chemical reduction, and biological techniques have been combined over the past few years [1, 2]. The biosynthesis of silver nanoparticles had advanced the use of microorganisms and chemical reduction method by using plant extracts [3, 4]. In this method, plants, being easily available, provide rapid and simple silver nanoparticle synthesis, due to the presence of metabolites consisting of terpenoids, vitamins, alkaloids, amino acids, enzymes,

proteins, etc., which act as both stabilizing and capping agents [5, 6]. The review of research studies revealed the generation of silver nanoparticles within the polymer network utilizing plant extract, notwithstanding biocompatible cellulose silver nanocomposites for antimicrobial, fabric, and therapeutic applications [7–9]. The *Xenostegia tridentata* (L.) possesses good diuretic, antiallergic, bitter, astringent, calefacient, laxative, purgative, fever, snake bite, tonic, and spasmolytic characteristics [10, 11]. *Xenostegia tridentata* (L.) leaf has been found to contain 3,5-caffeoylquinic acid, quercetin-3-o-rhamnoside, kaempferol-3-o-rhamnoside, luteolin-7-o-glucoside, β-sterol, and stigma sterol compounds that can be capping and reducing agents (XTLLs) which can easily reduce the silver nitrate solution to Ag ions in cellulose matrix [12–14]. In previous studies, the radical scavenging activities of silver nanoparticles and cellulose silver nanocomposites have been reported as a free radical scavenger in vivo and in vitro systems [15–17]. The literature suggests that silver nanoparticles and cellulose silver nanocomposites can treat cancer via alterations in cell morphology, cell viability, and lower metabolic activity [18–20]. In the past few decades, the fast development of the industry worldwide has critical environmental issues, especially water and soil contamination, which has harmed the biosphere [21]. Recently, Fan et al. prepared a self-assembled cellulose film having uniform Ag and tungsten oxide nanoparticles in cellulose matrix with the nanoparticles obtained by the reduction of polydopamine (PDA), previously deposited on cellulose for better adhesion of oxide nanoparticles. The flexible fiber showed excellent photocatalytic degradation of RB-19 dye with 93% efficiency under solar irradiation [22]. The nonsolvent-induced phase separation and in situ deposition technique was used to fabricate cellulose-Ag@AgCl-cellulose acetate/silk fibroin film, which showed excellent catalytic performance in the degradation of methyl orange dye. Ag nanoparticles enhanced the catalytic activity of the Ag@AgCl-CA/SF film [23, 24]. Junjie Wu et al. adopted an ecofriendly route to prepare porous cellulose/silver nanoparticle composite from NaOH/thiourea aqueous solution through sol-gel synthesis [25]. In this manuscript, we present an investigation on the in situ preparation of AgNPs in cellulose matrix to prepare cellulose silver nanocomposites Cell/XTLL/Ag NCs. The prepared Cell/XTLL/Ag NCs were characterized by TEM, SEM, FT-IR, XRD, UV-Vis spectroscopy, AFM, DRS, and TGA. ICP-OES was used for the measurements of silver nanoparticle concentration in the cellulose matrix. Eventually, this study investigates the antimicrobial cell viability test against human breast cancer cell line MCF-7, photocatalysis, and free radical scavenging properties of the novel Cell/XTLL/Ag NCs.

2. Materials and Methods

2.1. Plant Materials.
The plant material *Xenostegia tridentata* (L.) fresh leaves (Figure 1) have been accumulated from Ariyalur, Tamil Nadu, India.

The XTLL extraction leaves have been dried in the laboratory for six days at room temperature and then crushed into small pieces. The 20 g of XTLL (Figure 2(a)) was mixed with 300 ml of deionized water and heated to 82°C for 25 minutes, and then the solution was filtered and used (Figure 2(b)).

Figure 1: Leaves of *Xenostegia tridentata* (L.).

Figure 2: (a) *Xenostegia tridentata* (L.) leaf powder and (b) XTLL extract.

2.2. Chemicals.
The NaOH, 1,1-diphenyl-2-picrylhydroxyl, urea, and silver nitrate were purchased from Sigma Aldrich, Mumbai. 2, 2-Azino-bis(3-ethylbenzothiazoline-6-sulfonic acid) was purchased from Merck, Darmstadt, Germany. Degree of polymerization (Dp) of 620 (cotton linter) was supplied by Hubei Chemical Fiber, China.

2.3. Dissolution of Cellulose.
The technique described through [8, 26] was adopted; the aqueous solution was made up of mixing 8 wt% NaOH and 15 wt% of $CO(NH)_2$, with subsequent cooling to −13.0°C. This precooled solution was supplied with 5 wt% cotton linter pulp and was continuously stirred at high speed at room temperature. A clear solution of cellulose obtained under 3 min of stirring to the undissolved cellulose was removed by centrifugation at 7150 rpm and a temperature of 6°C for 15 min. The clear cellulose solution obtained was stored at 6°C for additional use.

2.4. Preparation of Cellulose/XTLL Composite Films.
The XTLL was dried in a warm air oven to remove the moisture; the dried leaf was added to cellulose solution and mixed thoroughly with the help of a mechanical stirrer. The cellulose solution was degassed to remove any air bubbles. Glass plates have been used for casting cellulose and cellulose/XTLL solution. The dried glass plates had been suspended in water and pH adjusted with

sulfuric acid; the regenerated composite films were washed thoroughly and kept immersed in the water bath until further use.

2.5. Preparation of Cellulose/XTLL Ag NC Composite Films.

The silver nitrate solutions at exclusive concentrations of 20, 40, and 60 mM were prepared; each of these solutions was kept taken separately and wet cellulose/XTLL composite films were immersed in each beaker and the whole arrangement was mixed thoroughly for 25 h. The color change of the wet films from light color to dark brown indicated the in situ generation of silver nanoparticles on the cellulose films. The wet films were washed and dried at room temperature and stored in desiccators for further use.

2.6. Sample Characterization.

The morphological studies of Cell/XTLL and Cell/XTLL Ag NCs have been executed with the usage of a SUPRA 55 Field Emission Scanning Electron Microscope from Carl Zeiss AG, Germany. The crystalline structure and morphology of Cell/XTLL Ag NCs have been additionally studied with the aid of using version TECNAI G2 FEI F12 TEM at a voltage of 200 kV. The X-ray diffractogram of the Cell/XTLL Ag NCs and cellulose has been recorded using the Bruker AXSD8 ADVANCE Diffractometer using Cu K-alpha radiation of 1.5406 A, U.S.A. Color change visualizations of the Cell/XTLL Ag NCs and the photocatalytic activity monitoring were carried out using the UV-1650PC, UV-visible spectrophotometer. To obtain FT-IR spectra, KBr and the nanocomposite have been pressure pressed to produce a disk, which was analyzed in the Avatar 330 FT-IR spectrophotometer. The size of silver nanoparticles was found using an AFM (model: Innova), Bruker AXS Pvt., Ltd., USA. A Thermo Fisher Scientific spectrometer using non-monochromatic Al K radiation 1486.5 eV run at 15 kV and 10 mA as an X-ray source was used to obtain the photoelectron spectra of the synthesized nanocomposites. The thermal gravimetric analyzer (TGA, Q50) was used to measure the weight loss and thermal behavior of the cellulose nanocomposite. The silver contents in the samples have been quantified by the usage of an inductively coupled plasma optical emission spectrophotometer with a cross-flow nebulizer and a Ryton Scott chamber.

2.7. Photocatalytic Activity Measurement.

The methylene blue was used as the model molecule to evaluate the photocatalytic activity of the prepared nanocomposites, Cell/XTLL and Cell/XTLL 60 mM AgNO$_3$. Typically, 0.05 g of the photocatalyst was introduced into 100 mL of 1.05 g L^{-1} dye solution. The mixture was dispersed in an ultrasonic bath for 15 min and then equilibrated in a dark room for 35 min. A black box, with a focus to attract sunlight, was used as an efficient illuminator for photocatalysis. Aliquots, of the reaction mixture, had been withdrawn and subjected to UV-Vis evaluation for studying the change in the absorbance of the peak at 640 nm. Repeated trials were conducted that had been completed to test the reusability of the photocatalysts (Cell/XTLL 60 mM AgNO$_3$).

2.8. Microorganisms.

The antimicrobial activities of Cellulose, Cell/XTLL, and Cell/XTLL—20, 40, and 60 mM AgNO3 have been investigated against antifungal and antibacterial activities which were procured from the Pondicherry Centre for Biological Sciences (PCBS), Pondicherry, India. The bacterial strains are *Escherichia coli* (MTCC 493), *Staphylococcus aureus* (MTCC 96), *Salmonella typhi* (MTCC 733), *Klebsiella* sp (ATCC 700834), and *Hafnia alvei* (ATCC 13337). The fungal strains are *Trichoderma viride* (ATCC 20476), *Fusarium oxysporum* (ATCC 48112), *Guignardia mangiferae* (ATCC 32759), *Aspergillus fumigates* (ATCC 1022), and *Candida albicans* (MTCC 227). The strain cultures had been grown in brain heart infusion liquid at 36 to 37°C; after 12 hours of undisturbed growth, each microorganism at a concentration of 1×106 cells/mL equivalent to 0.5 Mc Farland Standard was spread on the surface of Mueller–Hinton agar plates.

2.9. Preparation of Pathogens.

The pathogens to be tested had been spread on plates and a well with a 6 mm diameter made in the agar. The samples had been loaded in the concentration range from 45 to 55 µg/well compared with sterile antibiotics, which were loaded at the concentration of 22 µg/well. The samples had been incubated for 25 h, following which the zone of inhibition was measured and was regarded as the antimicrobial activity.

2.10. Free Radical Scavenging Activity.

The in vitro free radical scavenging activity of the nanocomposites with different silver concentrations was used: DPPH (2,2-diphenyl-1-picrylhydrazyl) and ABTS (2,2-azino-bis(3-etylbenzothiazoline-6-sulfonic acid) assays. The radical form of DPPH has an absorption band at 514 nm, which shall disappear upon reduction with the samples, demonstrating the antioxidant property. The photometric assay was settled by distributing the samples in different volumes in multiple test tubes. The total volume was adjusted to 10 µL using methanol; 5 mL of 0.1 methanolic solutions of DPPH was added and shaken vigorously. The solutions were equilibrated at 27°C. A control was also prepared with the procedure outlined above, but for the samples. Ascorbic acid ($C_6H_8O_6$) was used as an internal standard. The absorbance was measured at 516 nm and the percentage decolorization of the samples was calculated using the following formula, scavenging activity (%) = [(A517 of control −A517 of Cell/XTLL 20, 40, and 60 mM AgNO$_3$)/A517 of control] × 100. ABTS$^+$, 2, 2′-Azino-bis(3-ethyl-benzothiazoline-6−-sulfonic acid) scavenging activity: the assay was prepared by reacting a 7 mmol aqueous solution of ABTS$^+$, with 2.4 mM potassium persulfate in the dark for 12–16 h at 27°C. Care was taken to the prepared free radical solution to be stable for more than two days when stored in the dark at room temperature. During the absorbance measurement, 2 mL of the diluted free radical solution is added to the nanocomposite samples. Water was chosen as blank. After an incubation time of 36 minutes at room temperature, the absorbance was recorded at 732 nm and compared with ascorbic acid, the internal standard. The percentage of inhibition was calculated.

2.11. Anticancer Activity. Subculturing of cells: ahead of the experiment, the culture medium and TPVG (trypsin, PBS, Versene, and glucose solution) were brought to ordinary temperature. The tissue culture flask was pragmatic for cell degradation, pH, and turbidity, and a suitable flask was selected for splitting. In vitro evaluations were carried out using MCF-7 cell lines purchased from the National Centre for Cell Science (NCCS), Pune, and were used in this study. The subsequent procedure of progression is as follows: (1) the mouth of the flask was wiped with cotton soaked in spirit. (2) The medium was discarded and the cells had been washed twice, with MEM medium. (3) 4 mL of TVPG (prewarmed to 37°C) was added over the cells. (4) TPVG was allowed to act for $45 s^{-1}$ minute. (5) TPVG was discarded and 5 mL of 10% MEM was added. (6) The cell clusters were broken by gently pipetting (passaging the cells) back and forth. (7) 20 mL of growth medium was added to the tissue culture flask and the cells were transferred into 96 well plates. The calculation of the cell viability is carried out as % MCF-7 cell viability = absorbance at 540 of treated cells/ absorbance at 540 of control cells × 100%.

2.12. Statistical Analysis. The antibacterial, antifungal, DPPH, ABBTS, and cytotoxicity tests were performed in triplicate and repeated three times (mean ± SE). Statistical analysis was performed using the analysis of variance (ANOVA) method with Tukey's multiple comparison tests (Prism, version 5.0). The difference observed between samples was considered to be significant at $P < 0.05$ [27]. In the present work, Ag nanoparticles were produced in situ using Xenostegiatridentata (L.) leaf extract by changing the silver nitrate concentration (Cell/XTLL/20, 40, and 60 mM AgNO$_3$) in a polymer matrix.

3. Results and Discussion

These Cell/XTLL and Cell/XTL samples were examined using scanning electron microscopy and were exposed to 20, 40, and 60 mM AgNO$_3$ (Figures 3(a)–3(d)). The SEM photograph (Figures 3(b)–3(d)) shows the combination of mostly spherical Ag nanoparticles, located on the surface of the cellulose matrix; Figure 3(a) suggests the absence of spherical Ag nanoparticles on the cellulose matrix. The EDAX spectra were utilized to indicate that Ag metal was present in the Cell/XTLL20, 40, and 60 mM AgNO3 films, as shown in Figure 3(e) [9, 28].

The TEM image of Cell/XTLL 60 mM AgNO$_3$ had been observed to be a spherical shape as shown in Figures 4(a) and 4(b). The diameters of the silver nanoparticles were found to be around 33.78 nm, as presented in a histogram of particle size distribution (Figure 4(d)). The bright circular spots in the selected area electron diffraction (SAED) pattern (Figure 4(c)) show circular rings that can reveal the crystalline nature of the silver nanoparticles formed in cellulose matrix. Figure 4 reveals that the spherical Ag nanoparticles might be dispersed homogeneously on the surface of the cellulose matrix. In this case, the cellulose matrix (Cell/XTLL) serves as a capping, stabilizing, and reducing agent to the nanosized silver particles [29–31].

The X-ray diffraction spectra carried out by cellulose, Ag NPs, and Cell/XTLL 20, 40, and 60 mM AgNO$_3$ are shown in Figure 5. It was seen in our previous articles that in the case of raw cellulose, a broad peak appeared around 15.2° [32, 33]. In Figure 5, in Cell/XTLL 20.40, and 60 mM AgNO$_3$, the presence of Ag NPs is confirmed by peaks at $2\theta = 38°$, 44°, 64°, and 77° attributed to the crystallographic planes (3 1 1), (2 2 0) (2 0 0), and (1 1 1) of face-centered cubic silver crystals to be formed (JCPDS Card No. 893722-870720).

An FT-IR spectrum had been shown with the aid of using the presence of silver nanoparticles in the cellulose, XTL (leaf), as shown in Figures 6(a)–6(f). Cell/XTLLAgNO3 and Cell/XTL 20, 40, and 60 mMAgNO3 were the reactants used in the first reaction. In the XTLL extract and diffused cellulose, distinguished bands had been located at around 2258, 1719, 1625, 1557, and 1073 cm^{-1}. The observed bands account for C–O–C, C–O, and C=C organic functional groups. These bands can be attributed to 3,5-dicaffeoylquinic acid, quercetin-3-o-rhamnoside, kaempferol-3-o-rhamnoside, luteolin-7-o-glucoside, β-sterol, and stigmasterol compounds which might be considerably found in *Xenostegia tridentata* (L.) leaf extract [12–14] and are responsible for the reduction of silver ion to silver nanoparticles in the cellulose matrix.

It can be seen that an additional band at 1730 cm^{-1} was observed for the Cell/XTLL 60 mM AgNO$_3$ which was assigned to the C=O vibration as shown in Figure 6(c). It is evident that the carbonyl groups of XTLL were involved in the reduction of silver nitrate into silver nanoparticles in cellulose matrix. The cellulose used in this study has a high amount of hydroxyl (OH) groups as well as substantial inter- and intramolecular hydrogen (H) bonding interactions, characteristic of Cell/XTLL Ag NCs. These functional groups could be involved in the Ag NPs by anchoring Ag ions to the cellulose matrix and stabilizing the silver nanoparticles due to the interaction between cellulose hydrogen (H) bonds and the silver nanoparticles [9, 34, 35].

The XPS spectra evaluation is carried out further to confirm the chemical state of the cellulose silver nanoparticle composite. The survey spectra in Figure 7(a) clearly show the presence of oxygen (O1s) and carbon (C1s) from cellulose in nanocomposites. As shown in the inset of Figure 7(a), the XPS spectra clearly reveal the elemental status of Ag3d, which are doublet peaks formed by spin orbital coupling, Ag3d3/2 (371.51 eV) and Ag3d5/2 (366.3 eV). A high resolution analysis of Ag3d was performed for further investigation and the core level spectrum is shown in Figure 7(b). The spectrum deconvolutes into three components with binding energies of 368.3 eV (Ag$_2$O), 367.4 eV (AgO), and 366.3 eV (Ag^0), which can be assigned to Ag^0 corroborating the formation of silver nanoparticles on the surface of the cellulose [36–38].

Primarily, thermal stability of Cell/XTLL and Cell/XTLL Ag NCs was performed by TG for Cell/XTLL; there are mainly two weight loss stages below 160°C and 290 to 360°C (Figure 8) in which the first weight-loss stage corresponds to the evaporation of physically adsorbed water XTLL leaf extract which behaves as a reducing agent. The organic functional groups reduce their affinity toward moisture
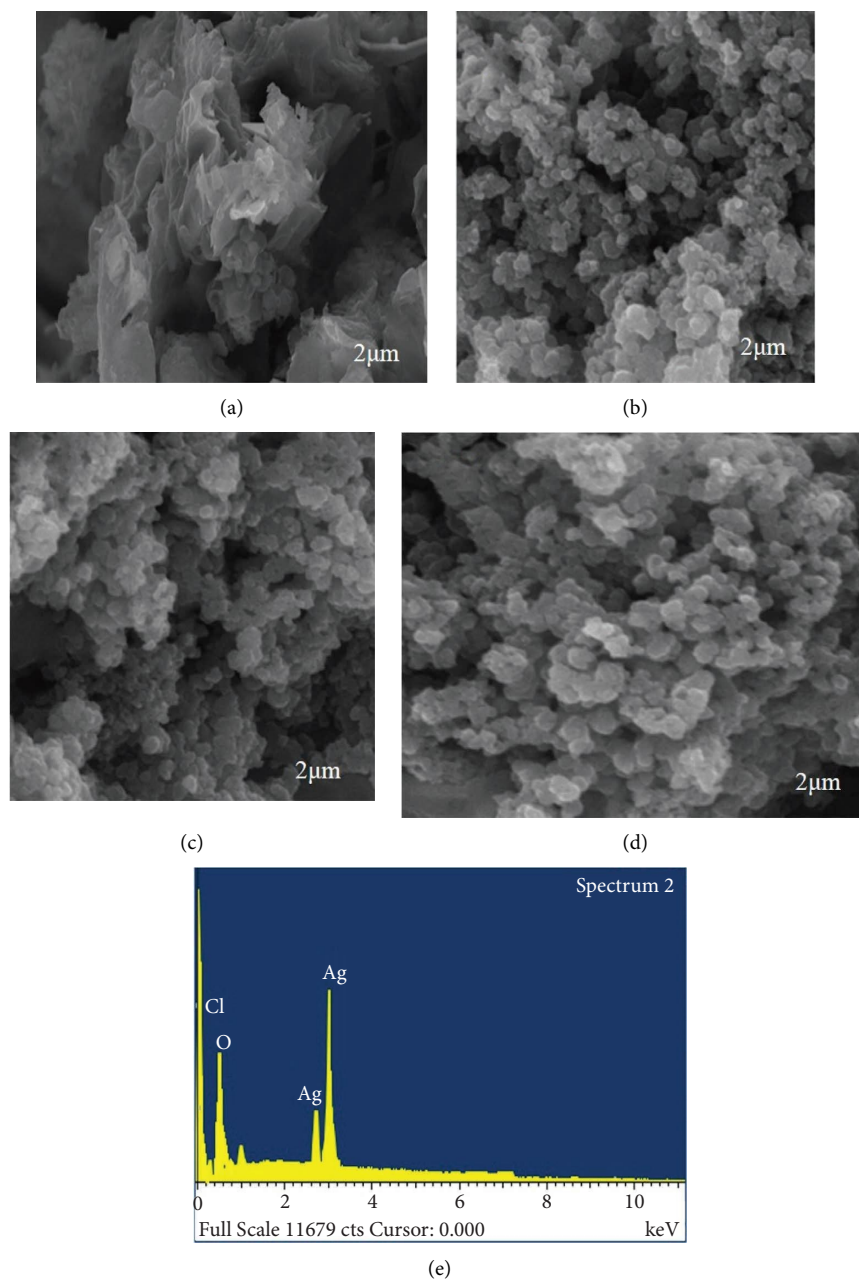
(a)   (b)

(c)   (d)

(e)

FIGURE 3: SEM images of (a) Cell/XTLL, (b) Cell/XTLL 20 mM AgNO$_3$, (c) Cell/XTLL 40 mM AgNO$_3$, (d) Cell/XTLL 60 mM AgNO$_3$, and (e) EDAX spectra of Cell/XTLL 60 mM AgNO$_3$.

absorption. As a result, a small quantity of water was absorbed by the surface of Cell/XTLL Ag NCs evaporated from the surface at a much lower temperature. In the second stage thermogram, the weight loss of about 87% is due to the decomposition of cellulose followed by carbonization. The nanocomposite (Cell/XTLL 60 mM AgNO$_3$) shows an overall weight loss of 64%, while the Cell/XTLL showed 97% decomposition. Hence, the deposition of silver nanoparticles resulted in a more thermal resistant material.

Using the first reaction mixture and the UV-Vis spectra of Cell/XTLL 20, 40, and 60 mM AgNO$_3$, it was observed that Ag nanoparticles are shown in Figure 9. It was demonstrated by the formation of a characteristic surface plasmon resonance absorption band at 415 to 425 nm; at this peak, it was confirmed that Ag ions present in the silver nitrate solution were reduced to silver nanoparticles. As the silver content increased, the peak intensity increased suggesting that the concentration of the silver nanoparticles also increased. The cellulose matrix is band-free, and the color shift from pale yellow to grey is all that is visible (Figure 10), indicative of redox reaction between the silver salt and carbonyl groups of XTLL. This grey color was persistent in the Cell/XTLL Ag NCs compound during four months of realization of the remaining experiments, suggesting that the cellulose used in this study provides good stability to the synthesized silver nanoparticles [39]. Both the solutions
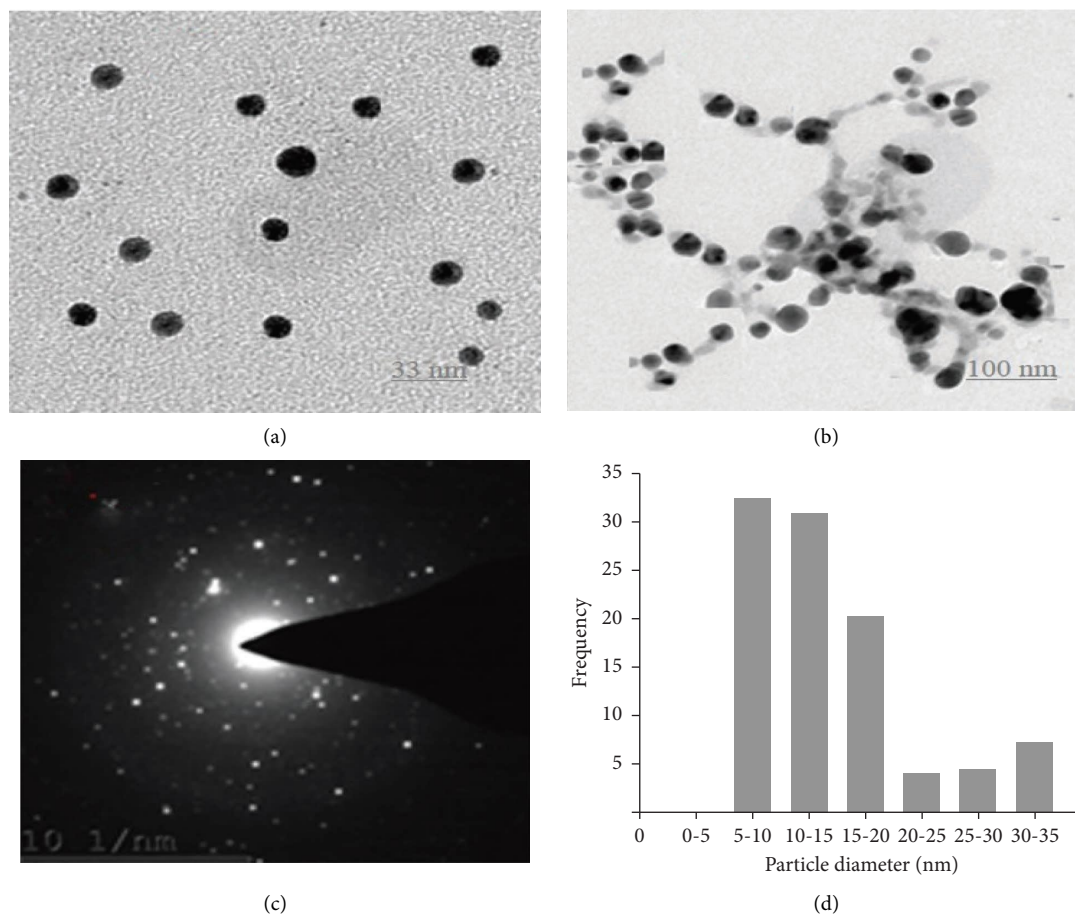
(a)

(b)

(c)

(d)

FIGURE 4: (a, b) TEM images of Cell/XTLL 60 mM AgNO$_3$, (c) SAED patterns of Cell/XTLL 60 mM AgNO$_3$, and (d) histogram of particle size distribution.
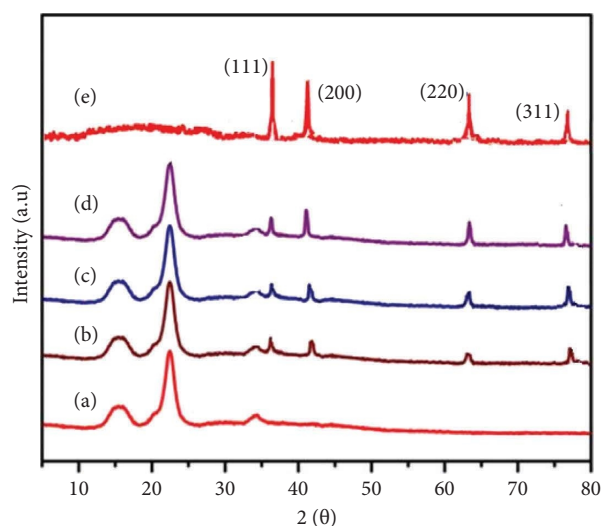

FIGURE 5: XRD spectra of (a) cellulose, (b) Cell/XTLL 20 mM AgNO$_3$, (c) Cell/XTLL 40 mM AgNO$_3$, (d) Cell/XTLL 60 mM AgNO$_3$, and (e) Ag NPs.

FIGURE 6: FTIR spectra of (a) cellulose, (b) XTLL, (c) starting reaction mixture of Cell/XTLL AgNO$_3$, (d) Cell/XTLL 20 mM AgNO$_3$, (e) Cell/XTLL 40 mM AgNO$_3$, and (f) Cell/XTLL 60 mM AgNO$_3$.

were withdrawn and further diluted to measure the Ag NP content using inductively coupled plasma optical emission spectr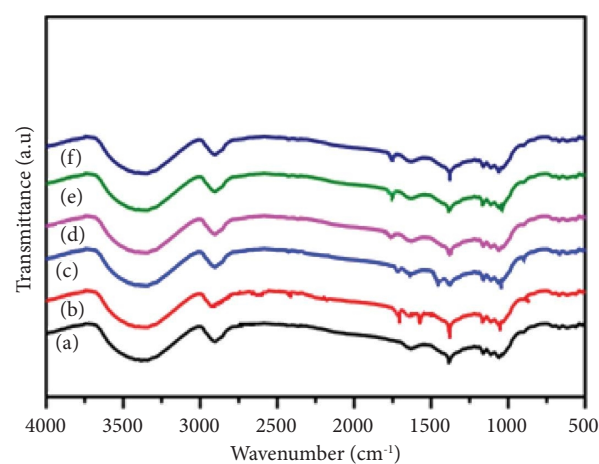oscopy and are listed in Table 1. It is observed that as the concentration of AgNO$_3$ solution increases, so does the formation of silver nanoparticles.

The UV-Vis reflection spectra of cellulose/XTLL and Cell/XTLL 20, 40, and 60 mM AgNO$_3$ are shown in
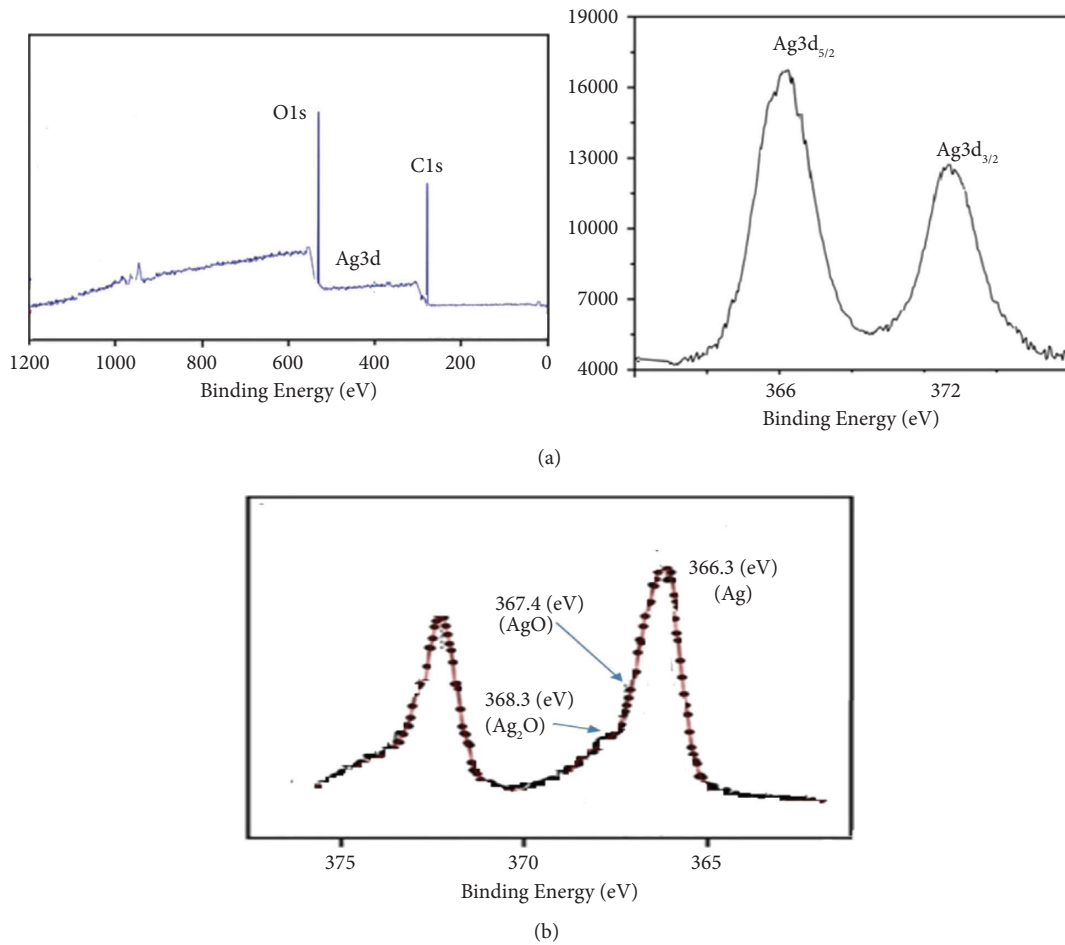
(a)

(b)

FIGURE 7: (a) XPS survey spectrum of Cell/XTL 60 mM AgNO$_3$ hybrids and (b) high resolution spectrum of Cell/XTL-60 mM AgNO$_3$.
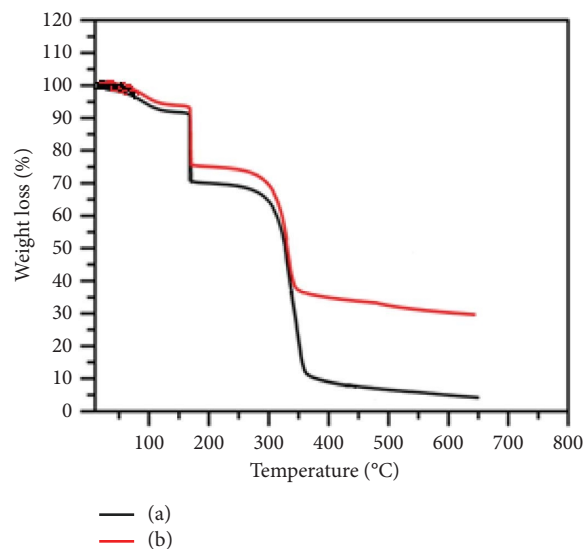

FIGURE 8: TGA spectra of (a) Cell/XTLL and (b) Cell/XTLL 60 mM AgNO$_3$.

Figure 11. These peaks are due to the surface plasmon effects due to the quantum confinement of Ag nanoparticles stabilized on the cell/XTLL surface. It can be observed that the strong absorption was seen between 400 and 500 nm. The Cell/XTLL 60 mM AgNO$_3$ band gap was calculated using the Kubelka–Munke equation and plotted as a function of
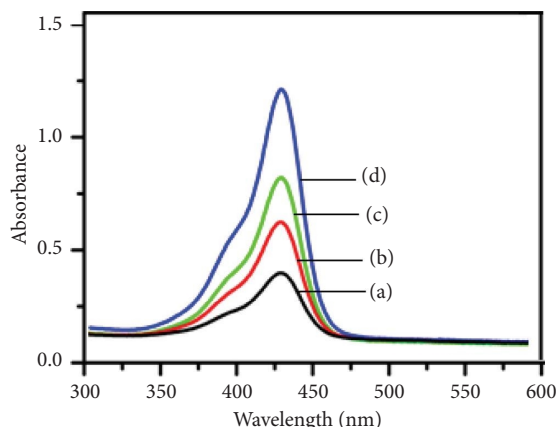
FIGURE 9: UV spectrum of (a) initial reaction mixture, (b) Cell/XTLL 20 mM AgNO$_3$, (c) Cell/XTLL 40 mM AgNO$_3$, and (d) Cell/XTLL 60 mM AgNO$_3$.
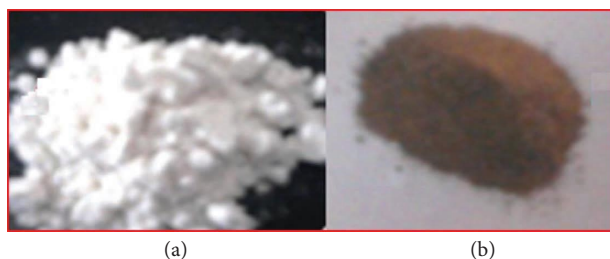

FIGURE 10: (a) Cellulose and (b) Cell/XTLL Ag NCs.

TABLE 1: ICP-OES analysis of Cell/XTLL and Cell/XTLL/20, 40, and 60 mM AgNO$_3$.

Samples	Ag NP content in Cell/XTLL Ag NCs (%)
Cell/XTLL	0
Cell/XTLL 20 mM AgNO$_3$	22
Cell/XTLL 40 mM AgNO$_3$	30
Cell/XTLL 60 mM AgNO$_3$	41

absorption coefficient versus band gap energy Cell/XTLL 60 mM AgNO$_3$. The band potentials of silver nanoparticles Ag (0) in the cellulose matrix were calculated theoretically and showed 3.40 eV at Cell/XTLL 60 mM AgNO$_3$ (Figure 11) [40].

The top morphology of the Cell/XTLL 60 mM AgNO$_3$ film was also characterized by atomic force microscopy. Figure 12 shows a 3D AFM image of the Cell/XTLL 60 mM AgNO$_3$ surface. The presence of silver nanoparticles on the cellulose surface can be observed as additional supporting evidence related to the surface roughness of Cell/XTLL 60 mM AgNO$_3$ at 33.78 nm which was evaluated (Figure 12). This result may indicate good adhesion and dispersion of Ag nanoparticles on the cellulose surface [41].

The antibacterial effects of cellulose, Cell/XTLL, Cell/AgNO$_3$, and Cell/XTLL 20, 40 mM AgNO$_3$, and Cell/XTLL-60 mM AgNO$_3$ against bacterial and fungal strains by disc diffusion tests are shown in Figures 13–16. It has been verified. It was observed that as the concentration of the silver nitrate solution increased, Ag NPs in the cellulose matrix increased and the inhibition zone also increased. *Escherichia coli*, *Staphylococcus aureus*, *Trichoderma viride,* and *Fusarium oxysporum* showed higher activity than the other microorganisms tested. Therefore, from the current approach, the developed Cell/XTLL 60 mM AgNO$_3$ can be regarded as an excellent antibacterial agent effective in killing microorganisms. It can also be concluded that the developed Cell/XTLL 60 mM AgNO$_3$ nanocomposites have a larger inhibition zone compared to other prepared nanocomposites. Cellulose-silver nanocomposites penetrate more effectively into bacterial and fungal cells, damaging cell nuclei and killing fungi faster. The primed Cell/XTLL Ag NCs can penetrate the bacterial cell wall and induce cell death. Cell/XTLL Ag NCs can increase the permeability of cell membranes. The production of reactive oxygen species releases Ag ions and interferes with the replication of deoxyribonucleic acid [42–44].

The DPPH and ABTS$^+$ free radical scavenging ability of cellulose, Cell/XTLL, Cell/AgNO$_3$, Cell/XTLL/20, 40, and 60 mM AgNO$_3$, and ascorbic acid (standard) indicated that their DPPH activity was dose-dependent, with increased inhibition of 2.34, 4.23, 11.85, 55.76, 71.58, 82.31, and 85.12% (ascorbic acid) at 40 μg/mL, respectively (Table 2 and Figure 17). The prepared Cell/XTLL 60 mM AgNO$_3$ is effective against DPPH radicals. Absorption rates of ABTS$^+$ radicals from cellulose, Cell/XTLL, Cell/AgNO$_3$, and cellulose-silver nanoparticles increased by approximately 2.87, 3.92, 10.31, 53.23, 62.87, 73.53, and 75.45% (ascorbic acid) (Table 3 and Figure 18). The Cell/XTLL 60 mM AgNO$_3$, the most powerful nanocomposite (Cell/XTLL 20, 40, and 60 mM AgNO$_3$), increases silver nanoparticles in the cellulose matrix and blocks DPPH as the concentration of silver nitrate solution increases. Due to the increase, it provided the highest DPPH and ABTS$^+$ activity and ABTS$^+$. This may indicate a combined effect of silver nanoparticles and XTLL in the cellulose matrix that significantly binds DPPH and ABTS$^+$ [17, 45].

The cancer activity of Cell/XTLL 20, 40, and 60 mM AgNO$_3$ on MCF-7 cells was determined by the MTT assay [46], when MCF-7 cells (1×105/well) were plated in 0.2 ml
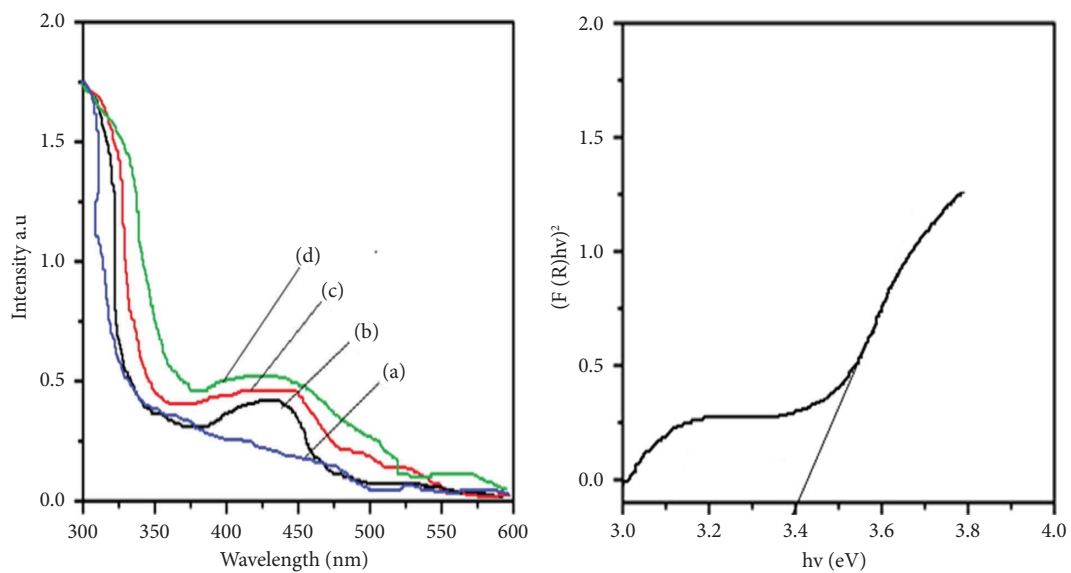
FIGURE 11: Diffused reflectance spectra of (a) Cell/XTLL, (b) Cell/XTLL 20 mM AgNO$_3$, (c) Cell/XTLL 40 mM AgNO$_3$, and (d) Cell/XTLL 60 mM AgNO$_3$, and plot for band gap calculation, Cell/XTLL 60 mM AgNO$_3$.
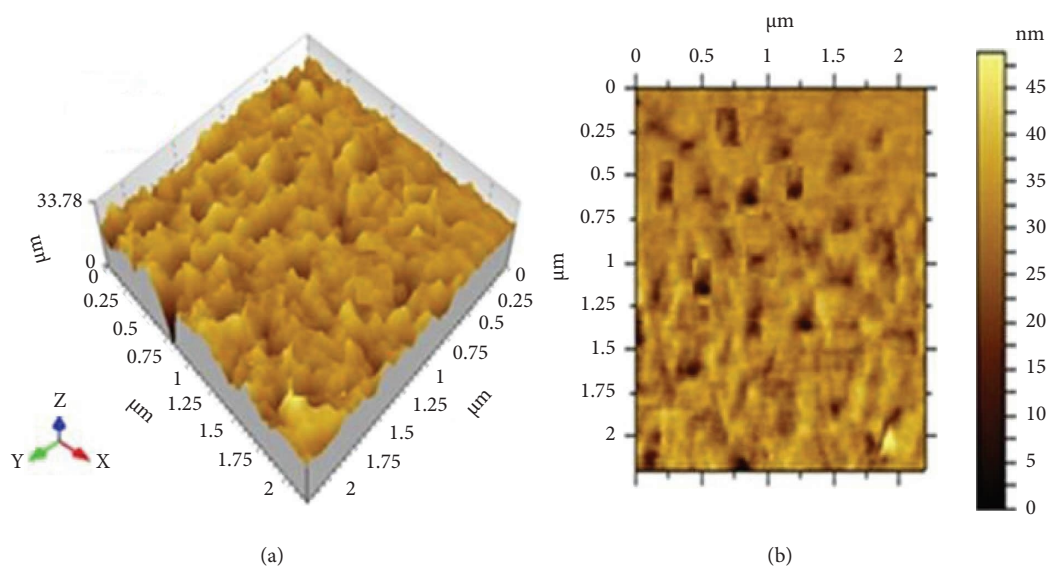

(a)

(b)

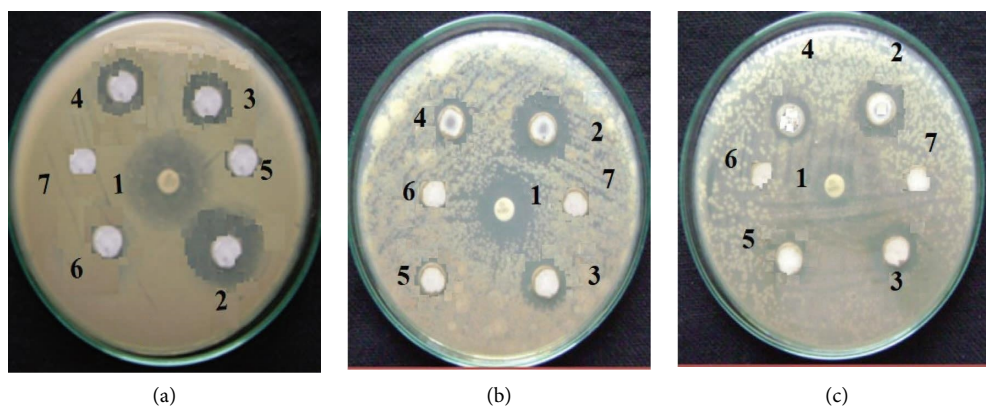FIGURE 12: AFM images: (a) three dimensional and (b) two dimensional of Cell/XTLL 60 mM AgNO$_3$.

(a)

(b)

(c)

FIGURE 13: Continued.

(d)

(e)

FIGURE 13: Antibacterial activity of cellulose (7), Cell/XTLL (6), Cell/AgNO$_3$ (5), and Cell/XTLL Ag NCs (20 (4), 40 (3), and 60 (2) mM AgNO$_3$) and positive control ciprofioxacin (1). Bacteria strains: *Escherichia coli* (a), *Staphylococcus aureus* (b), *Salmonella typhi* (c), *Klebsiella sp* (d), and *Hafnia alvei* (e).

FIGURE 14: Antibacterial activity of cellulose, Cell/XTLL, Cell/AgNO$_3$, and Cell/XTLL Ag NCs (20, 40, and 60 mM AgNO$_3$). Asterisk (*) denotes a significant difference compared to control ($P < 0.05$).

(a)   (b)   (c)
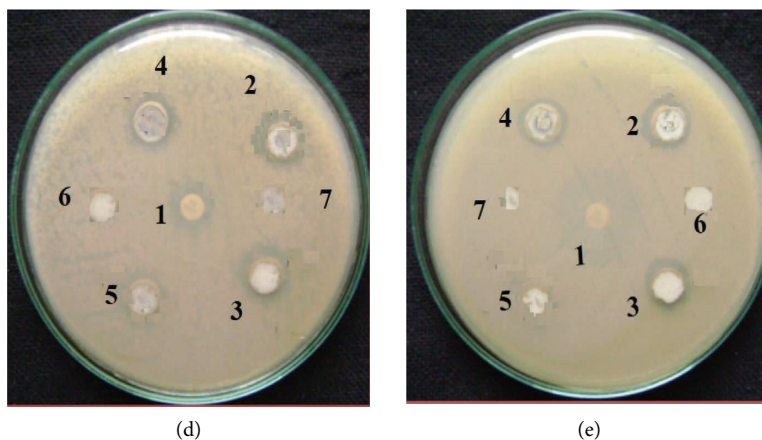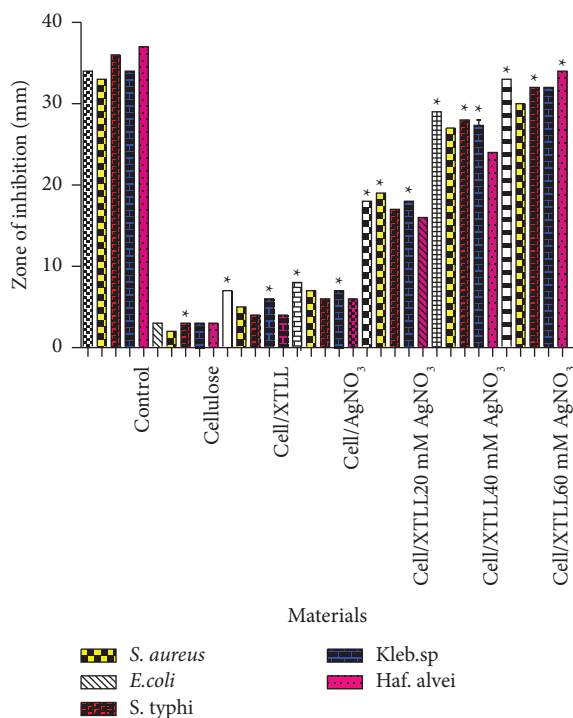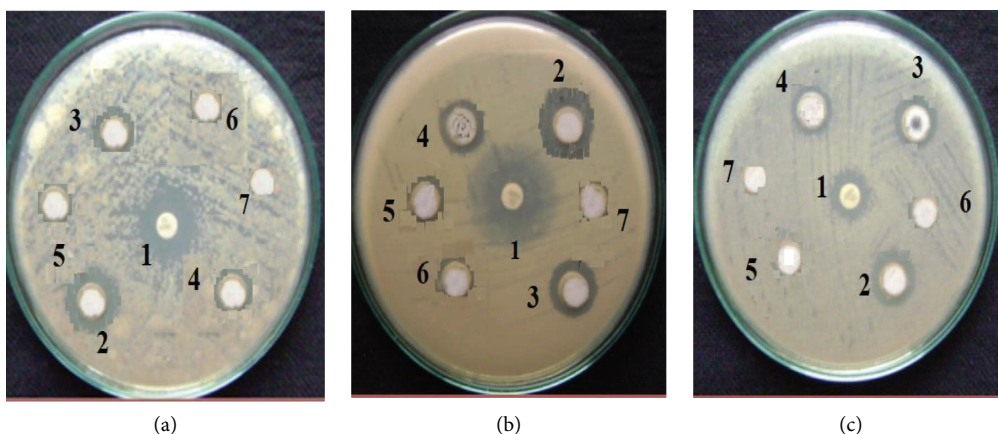
FIGURE 15: Continued.

(d)

(e)

FIGURE 15: Antifungal activity of cellulose (7), Cell/XTLL (6), Cell/AgNO$_3$ (5), and Cell/XTLL Ag NCs (20 (4), 40 (3), and 60 (2) mM AgNO$_3$ and positive control ciprofioxacin (1). Fungal strains: *Trichoderma viride* (a), *Fusarium oxysporum* (b), *Guignardia mangiferae* (c), *Aspergillus fumigatus* (d), and *Candida albicans* (e).
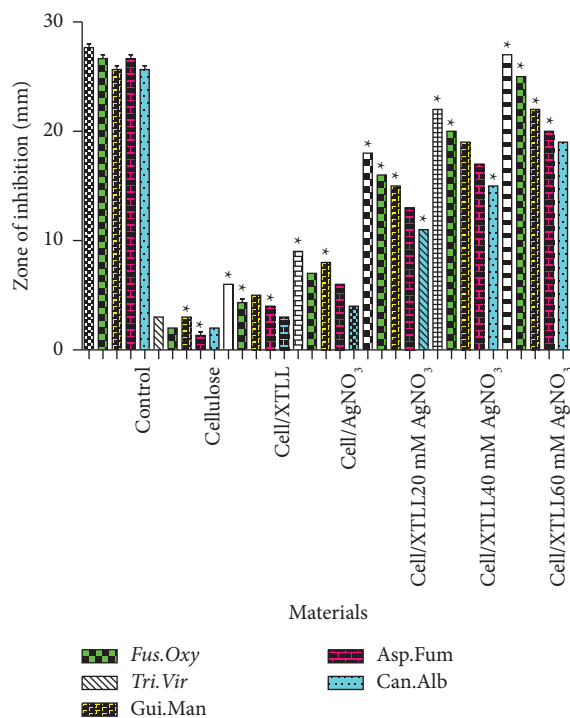
FIGURE 16: Antifungal activity of cellulose, Cell/XTLL, Cell/AgNO$_3$, and Cell/XTLL Ag NCs (20, 40, and 60 mM AgNO$_3$). Asterisk (*) denotes a significant difference compared to control ($P < 0.05$).
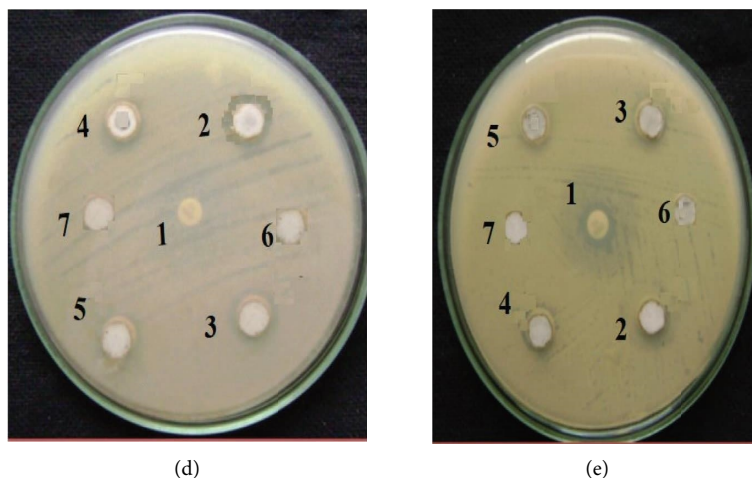
medium/well on a 95-well plate and incubated in a 5% CO$_2$ incubator for 72 hours. Then, various concentrations of the Cell/XTLL 20, 40, and 60 mM AgNO$_3$ at various concentrations in 0.1% DMSO were added and placed at a 5% CO$_2$ incubator for 24 h. The MCF- cells were observed under an inverted microscope at a magnification of 40X and

TABLE 2: Effect of Cellulose, Cell/XTLL, Cell/AgNO$_3$, and Cell/XTLL 20, 40, and 60 mM AgNO$_3$ on DPPH assay.

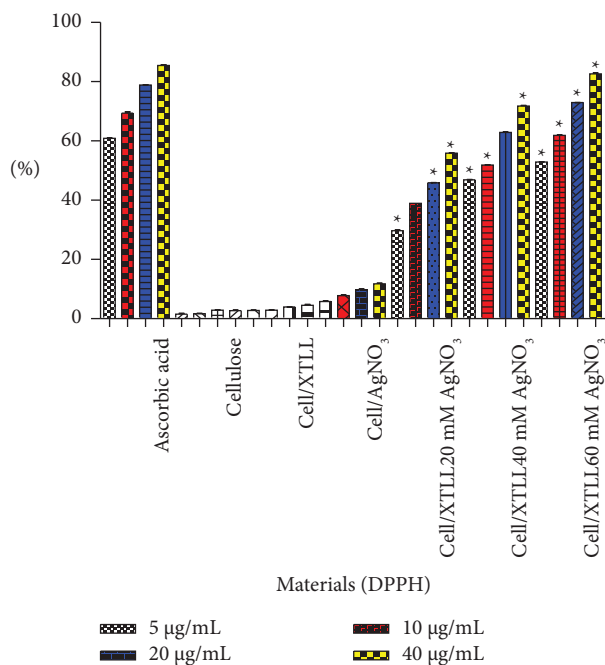| Different concentrations	Cellulose	Cell/XTLL	Cell/AgNO$_3$	Cell/XTLL 20 mM AgNO$_3$	Cell/XTLL 40 mM AgNO$_3$	Cell/XTLL 60 mM AgNO$_3$	Ascorbic acid
Conc 5 μg/ml	1.26	2.64	5.35	29.32	46.82	52.67	60.76
Conc 10 μg/ml	1.46	2.96	7.34	38.98	51.87	61.83	69.36
Conc 20 μg/ml	2.76	3.24	9.34	45.76	62.86	72.95	78.69
Conc 40 μg/ml	2.34	4.23	11.85	55.76	71.58	82.31	85.12

FIGURE 17: Effect of cellulose, Cell/XTLL, Cell/AgNO$_3$, and Cell/XTLL Ag NCs (20, 40, and 60 mM AgNO$_3$) on DPPH assay. Asterisk (*) denotes a significant difference compared to control ($P < 0.05$).

the images were recorded. After removing the Cell/XTLL 20, 40, and 60 mM AgNO$_3$ solution, 20 μl/well MTT reagents were added; viable MCF-7 cells were determined by the absorbance at 540 nm. A 50% inhibition of cell viability (IC50) value was graphically determined. The effect of Cell/XTLL 20, 40, and 60 mM AgNO$_3$ on MCF-7 cell proliferation was expressed as cell viability using the following equation: % MCF-7 cell viability = A540 treated cells/A540 control cells × 100%. Cell/XTLL 20, 40, and 60 mM AgNO$_3$ were tested for potential inhibitory effects on human breast cancer cell proliferation in MCF-7 cervical cancer cell lines using the MTT assay shown in Figure 19.

The cytotoxic effects of Cell/XTLL 20, 40, and 60 mM AgNO$_3$ on MCF-7 cervical cancer cell lines at 72 hours at different concentrations shown in Figures 19(A)–19(D) may be deduced that for cell lines, cell count decreases as sample concentration increases (Table 4). In this process, silver nanoparticles in the Cell/XTLL Ag NCs bind and penetrate the negatively charged cancer cell to disturb metabolic and membrane activity leading to cell death. The Cell/XTLL Ag NCs also release positively charged (Ag$^+$) cation which leads to the destruction of the cell wall. The prepared Cell/XTLL Ag NCs are endocytosed into MCF-7 cells; this can release their cargo to exert a therapeutic effect. However, the strength of this interaction depends not only on the rate of endocytosis but also on the residence time and accumulation of the silver nanoparticles inside cells [47].

Photocatalytic activity of cellulose-silver nanocomposites: the absorption intensity of MB at 525 nm decreased with increasing irradiation time, indicating that the concentration of MB dye also decreased with

increasing irradiation time as shown in Figures 20(a) and 20(b). When exposed to light, photon absorption occurs, and (e$^-$h$^+$) charge loss occurs due to the excitation of electrons (e$^-$) from the valence band of silver nanoparticles and the abandonment of the conduction band opening to do a band of silver nanoparticles [48–51]. Photocatalytic tests have shown that UV light and catalytic activity are required to effectively destroy MB. The pure Cell/XTLL and Cell/XTLL 60 mM AgNO$_3$ nanocomposites were used under equivalent conditions with only 49% and 91% degradation, respectively. This shows that the Cell/XTLL 60 mM AgNO$_3$ nanocomposite process can handle MB degradation better than other prepared nanocomposites. Degradation was more successful with Cell/XTLL 60 mM AgNO$_3$ nanocomposites, but we investigated the effects of valid parameters in this process and found optimal conditions.

In catalytic decomposition, the pseudofirst-order rate constants (plot ln (C/C$_0$) vs. time t) show a linear relationship, as shown in Figure 20(c), where C is the concentration of MB dye. When integrated within the range of C/C$_0$ at $t = 0$, C$_0$ is the equilibrium concentration of the bulk solution of the MB dye, and the formula (ln (C/C$_0$) = k_t) is obtained, where C$_0$ is the equilibrium concentration of the dye. Solution, C = concentrations and t = time; therefore, the equation has the following form ln (C$_0$/C) = $K_{App}t$, where K_{App} (min^{-1}) is the first-order pseudodynamics of the velocity constant shown Figure 18(d), $t/q_t = 1/k_2$ qe$_2$ + t/qe velocity constant second reaction rate Figure 20(d). The rate constant values for photocatalytic decomposition of MB dye by Cell/XTLL and Cell XTLL 60 mM AgNO$_3$ were found to

Table 3: Effect of Cellulose, Cell/XTLL, Cell/AgNO$_3$, and Cell/XTLL 20, 40, and 60 mM AgNO$_3$ on ABBTS$^+$ assay.

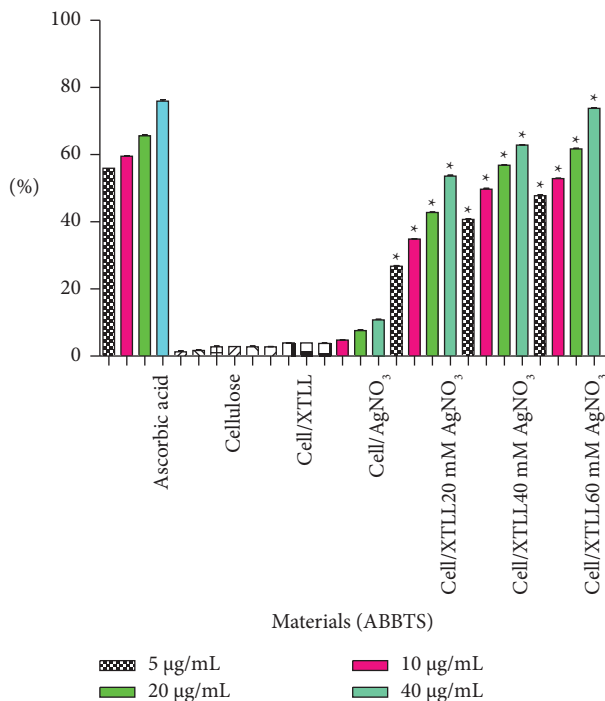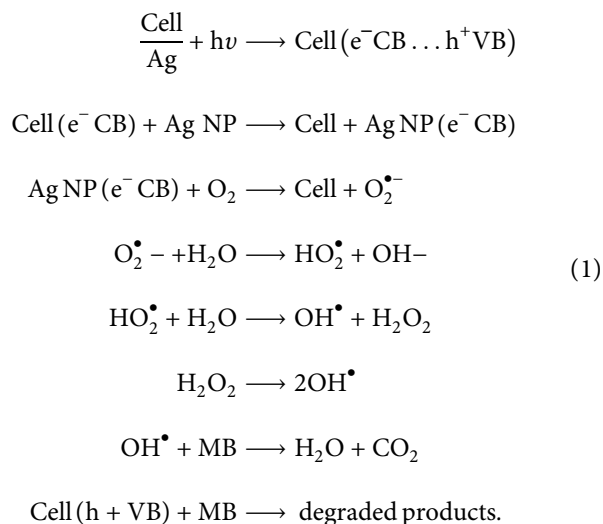| Different concentrations	Cellulose	Cell/XTLL	Cell/AgNO$_3$	Cell/XTLL 20 mM AgNO$_3$	Cell/XTLL 40 mM AgNO$_3$	Cell/XTLL 60 mM AgNO$_3$	Ascorbic acid
Conc 5 μg/ml	1.01	2.41	3.6	26.47	40.45	47.34	55.98
Conc 10 μg/ml	1.36	2.57	4.6	34.97	49.21	52.86	59.29
Conc 20 μg/ml	2.59	3.87	7.3	42.65	56.92	61.67	65.32
Conc 40 μg/ml	2.87	3.92	10.31	53.23	62.87	73.53	75.45

FIGURE 18: Effect of cellulose, Cell/XTLL, Cell/AgNO₃, and Cell/XTLL-Ag NCs (20, 40, and 60 mM AgNO₃) on ABTS⁺ assay. Asterisk (*) denotes a significant difference compared to control ($P < 0.05$).

be $k = 0.9723$ and $k = 0.94242$, respectively. The proposed mechanism of photocatalytic activity of the cell/XTLL 60 mM AgNO₃ heterojunction nanocomposites is outlined in Figure 21 as charge transfer and energy position. Cellulose is common, has a large surface area, and has a loose porous structure, so it can absorb large amounts of contaminants in a dark environment and balance absorption and desorption. This is because the photo-generated electrons on the Ag conduction band can be transferred to the conductive network system on the Cell/XTLL composite due to the conductivity that prevents the photo-generated electrons and holes from binding. As a result, the addition of AgNO₃ to the fabric significantly improved the photocatalytic properties. In addition, the introduction of AgNO₃ nanoparticles separates electrons and holes by absorbing visible light through the SPR effect. In addition, electrons or holes transferred to the nanostructure Cell/XTLL 60 mM AgNO₃ active surface are directly involved in the redox reaction. In this reaction, the electrons reduce the dissolved oxygen to mimic the superoxide anion (O_2^-), and the H_2O^- the molecule is oxidized to provide hydroxyl radical (OH). Organic dye contaminants (MBs) are eventually oxidized to CO_2 and H_2O products by these highly elastic species. Apart from hydroxyl radicals, holes have been identified as the most

important active species in the Cell/XTLL 60 mM AgNO₃ system [52, 53]. The grafted silver nanoparticles can act as preferred hole channels and receptors for efficient separation of photo-excited electrons and holes, thereby enhancing the photocatalytic properties of Cell XTLL 60 mM AgNO₃ shown as follows:

$$
\begin{aligned}
\frac{\text{Cell}}{\text{Ag}} + h\nu &\longrightarrow \text{Cell}\left(e^- \text{CB} \dots h^+ \text{VB}\right) \\
\text{Cell}\left(e^- \text{CB}\right) + \text{Ag NP} &\longrightarrow \text{Cell} + \text{Ag NP}\left(e^- \text{CB}\right) \\
\text{Ag NP}\left(e^- \text{CB}\right) + O_2 &\longrightarrow \text{Cell} + O_2^{\bullet-} \\
O_2^{\bullet} - + H_2O &\longrightarrow HO_2^{\bullet} + OH- \\
HO_2^{\bullet} + H_2O &\longrightarrow OH^{\bullet} + H_2O_2 \\
H_2O_2 &\longrightarrow 2OH^{\bullet} \\
OH^{\bullet} + MB &\longrightarrow H_2O + CO_2 \\
\text{Cell}\left(h + VB\right) + MB &\longrightarrow \text{ degraded products.}
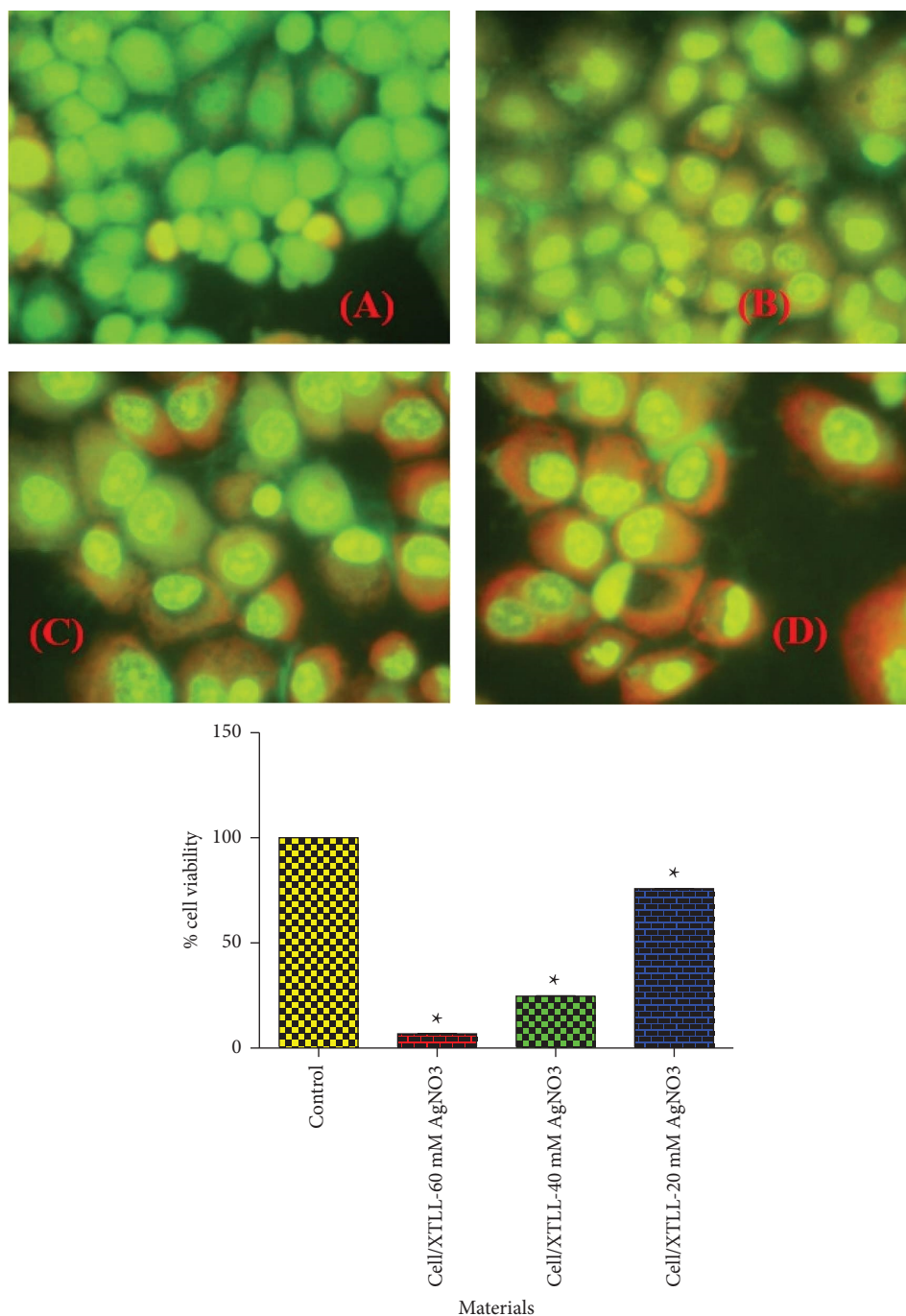\end{aligned}
\tag{1}
$$

Figure 19: Cytotoxic effect of Cell/XTLL Ag NCs: (A) control MCF-7 cell line, (B) Cell/XTLL 20 mM AgNO$_3$, (C) Cell/XTLL 40 mM AgNO$_3$, and (D) Cel/XTLL 60 mM AgNO$_3$. Asterisk (*) denotes a significant difference compared to control (0.05).

Table 4: Cytotoxic effect of Cell/XTLL 20, 40, and 60 mM AgNO$_3$ on MCF-7 cell lines at 72 hours.

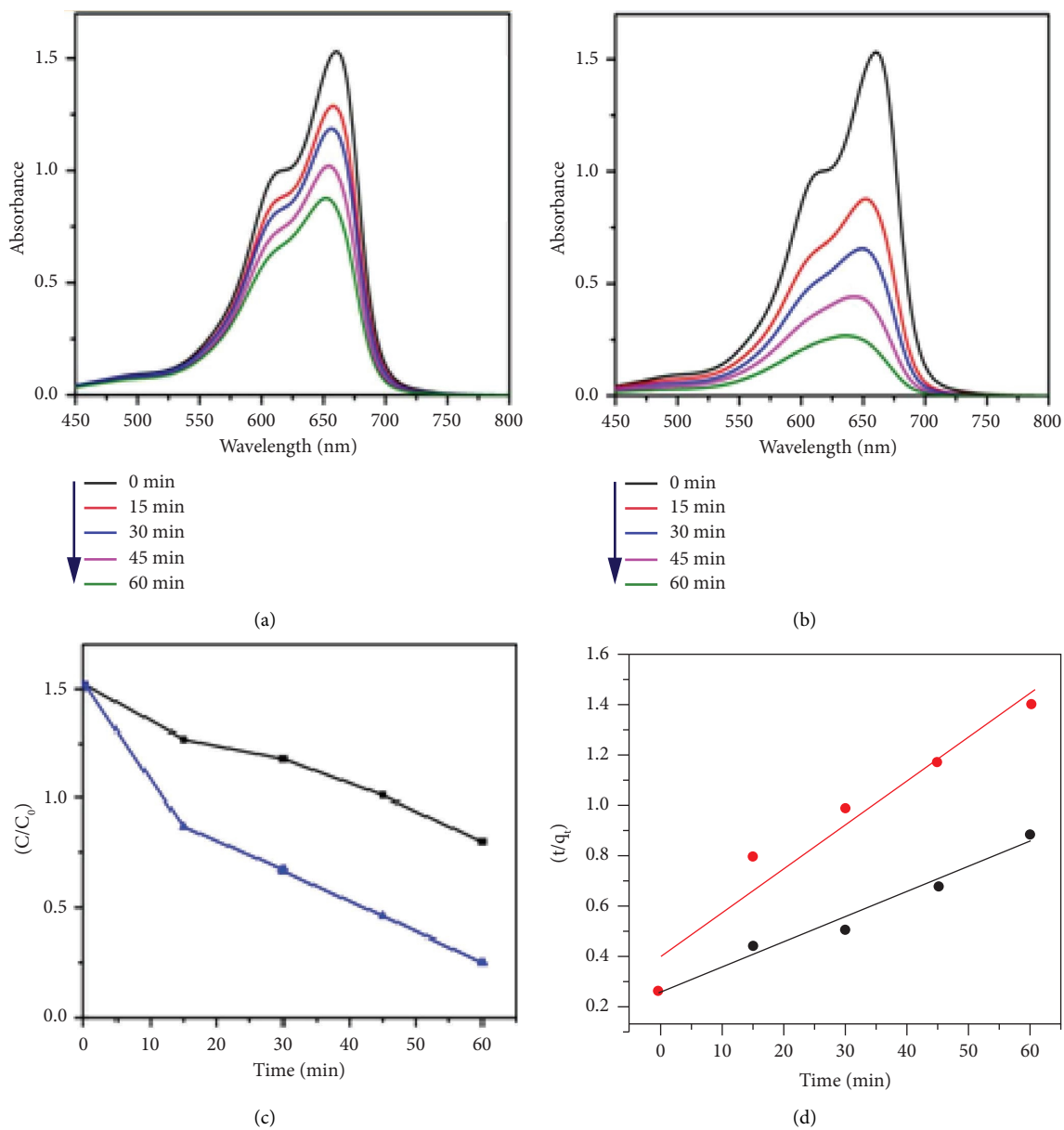| S. no.	Cytotoxic effect of cell/XTLL/20, 40, and 60 mM AgNO$_3$ μg/ml on MCF-7 cell line	Absorbance 540 nm	% cell viability
1	Cell/XTLL 60 mM AgNO$_3$	0.08	6.7
2	Cell/XTLL 40 mM AgNO$_3$	0.27	24.6
3	Cell/XTLL 20 mM AgNO$_3$	0.85	75.8
4	Control cell	1.17	100

FIGURE 20: Photocatalytic activity of MB dye: (a) Cell/XTLL, (b) Cell/XTLL 60mM AgNO3, (c) degradation efficiency, and (d) pseudofirst-order kinetics.
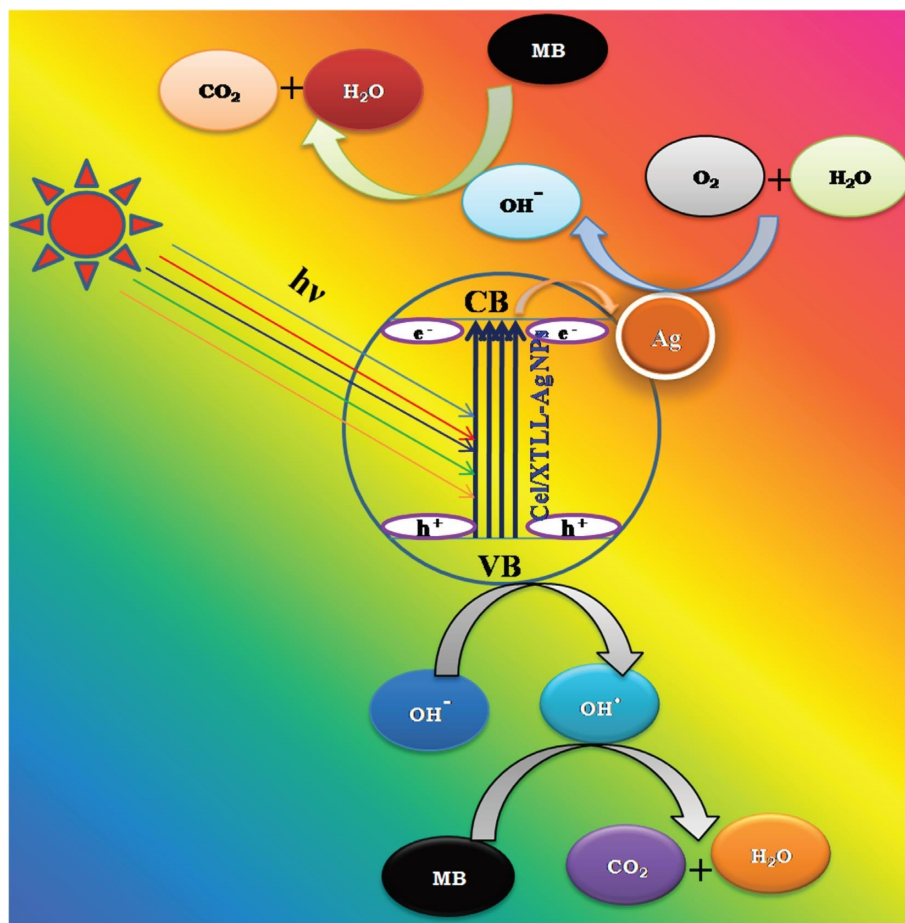
Figure 21: Schematic diagram of photocatalytic mechanism of Cell/XTLL 60mM AgNO$_3$.

4. Conclusion

In summary, *Xenostegia tridentata* (L.) leaf extract is used as a reducing agent and silver nitrate is used as a silver precursor, environmentally friendly green synthesis, to produce silver nanoparticles (in situ) in a cellulose matrix. The SEM and TEM results show that the spherical shape silver nanoparticles are evenly dispersed in the Cell/XTLL matrix. The XPS spectra observed that the Ag^{3}d$^{5/2}$ peak was composed at 368.82 eV, which can be assigned to Ag^0. Among these are the XRD patterns of face-centered cubic silver in cellulose matrix (3 1 1), (2 2 0), (2 0), and (1 1 1). The FT-IR spectra were concluded that C– O–C, C–O, and C = C functional groups reducing silver ion to Ag nanoparticles. The most potent have been synthesized Cell/XTLL 60 mM AgNO3 against Escherichia coli, Staphylococcus aureus, Trichoderma viride, and Fusarium oxysporum have strong antimicrobial activity, DPPH, ABTS+ scavengers, and MTT assay for its highly inhibitory effect on human tumor cell proliferation in MCF-7 cervical cancer cell lines. In this cellulose-silver nanocomposite heterojunction nanostructure, Ag may (i) enhance the composite's response to visible light and (ii) enhance fast electron transfer and inhibit charge recombination. Consequently, the synthesis of highly photocatalytic 1D cellulose silver nanocomposites opens up a wider range of applications which can be effectively used as a photocatalyst to decompose organic pollutants in aqueous bodies, thereby helping to restore the environment.

Data Availability

The data used to support the study are available from the corresponding author upon request.

Conflicts of Interest

The authors declare that there are no conflicts of interest.

Acknowledgments

References

[1] S. Iravani, H. Korbekandi, S. V. Mirmohammadi, and B. Zolfaghari, "Synthesis of silver nanoparticles: chemical, physical and biological methods," *Research in Pharmaceutical Sciences*, vol. 9, no. 6, pp. 385–406, 2014.

[2] H. Wang, X. Qiao, J. Chen, and S. Ding, "Preparation of silver nanoparticles by chemical reduction method," *Colloids and Surfaces A: Physicochemical and Engineering Aspects*, vol. 256, no. 2-3, pp. 111–115, 2005.

[3] K. Gudikandula, P. Vadapally, and M. Singara Charya, "Biogenic synthesis of silver nanoparticles from white-rot Fungi: their characterization and antibacterial studies," *Open Nano*, vol. 2, pp. 64–78, 2017.

[4] S. Rajput, D. Kumar, and V. Agrawal, "Green synthesis of silver nanoparticles using Indian *belladonna* extract and their potential antioxidant, anti-inflammatory, anticancer and larvicidal activities," *Plant Cell Reports*, vol. 39, no. 7, pp. 921–939, 2020.

[5] A. Roy, O. Bulut, S. Some, A. K. Mandal, and M. D. Yilmaz, "Green synthesis of silver nanoparticles: biomolecules-nanoparticles organizations targeting antimicrobial activity," *RSC Advances*, vol. 9, no. 5, pp. 2673–2702, 2019.

[6] S. F. Hashemi, N. Tasharrofi, and M. M. Saber, "Green synthesis of silver nanoparticles using *teucrium polium* leaf extract and assessment of their antitumor effects against MNK45 human gastric cancer cell line," *Journal of Molecular Structure*, vol. 1208, Article ID 127889, 2020.

[7] A. Fadakar Sarkandi, M. Montazer, T. Harifi, and M. Mahmoudi Rad, "Innovative preparation of bacterial cellulose/silver nanocomposite hydrogels: in situ green synthesis, characterization, and antibacterial properties," *Journal of Applied Polymer Science*, vol. 138, no. 6, Article ID 49824, 2020.

[8] M. Kishanji, G. Mamatha, K. Obi Reddy, A. Varada Rajulu, and K. Madhukar, "In situ generation of silver nanoparticles in cellulose matrix using *azadirachta indica* leaf extract as a reducing agent," *International Journal of Polymer Analysis and Characterization*, vol. 22, no. 8, pp. 734–740, 2017.

[9] C. Shanmugam, G. Sivasubramanian, P. Govindhan, P. Bera, K. Baskaran, and V. R. Parameswaran, "Antimicrobial and free radical scavenging activities of Cellulose/Silver-Nanocomposites with in situ generated silver nanoparticles using *Cissampelos pareira* leaf extract," *Journal of Cluster Science*, vol. 33, no. 4, pp. 1727–1737, 2021.

[10] D. F. Austin and G. W. S. Iii, "Xenostegia, a new genus of convolvulaceae," *Brittonia*, vol. 32, no. 4, pp. 533–536, 1980.

[11] D. F. Austin, "Sendera-clandi (Xenostegia tridentate (L) D.F, Austin & Staples, convolvulaceae): a medicinal creeper," *Ethnobotany Research and Applications*, vol. 12, pp. 433–454, 2014.

[12] R. Suntivich, W. Songjang, A. Jiraviriyakul, S. Ruchirawat, and J. Chatwichien, "LC-MS/MS metabolomics-facilitated identification of the active compounds responsible for anti-allergic activity of the ethanol extract of *Xenostegia tridentate*," *PLoS One*, vol. 17, no. 4, Article ID e0265505, 2022.

[13] R. Govaerts, "Xenostegia tridentate in world checklist of selected plant families," *The board of trustees of the royal botanic gardens*, 2019.

[14] M. S. M. Sosef, R. E. Gereau, S. B. Janssens, M. Kompanyi, and A. R. Simões, "A curious new species of *Xenostegia (convolvulaceae)* from central Africa, with remarks on the phylogeny of the genus," *Systematic Botany*, vol. 44, no. 2, pp. 405–414, 2019.

[15] J. Banerjee and R. T. Narendhirakannan, "Biosynthesis of silver nanoparticles from *Syzygiumcumini L* seed extract and evaluation of their in vitro antioxidant activities," *Digest Journal of Nanomaterials and Biostructures*, vol. 6, pp. 961–968, 2011.

[16] R. Konwarh, B. Gogoi, R. Philip, M. A. Laskar, and N. Karak, "Biomimetic preparation of polymer-supported free radical scavenging, cytocompatible and antimicrobial green silver nanoparticles using aqueous extract of *citrus sinensis peel*," *Colloids and Surfaces B: Biointerfaces*, vol. 84, no. 2, pp. 338–345, 2011.

[17] Z. Bedlovičová, I. strapac, M. Baláž, and A. Salayova, "A brief overview on antioxidant activity determination of silver nanoparticles," *Molecules*, vol. 25, no. 14, p. 3191, 2020.

[18] T. Q. Huy, P. T. M. Huyen, A. T. Le, and M. Tonezzer, "Recent advances of silver nanoparticles in cancer diagnosis and treatment," *Anti-Cancer Agents in Medicinal Chemistry*, vol. 20, no. 11, pp. 1276–1287, 2020.

[19] A. C. Gomathi, S. R. Xavier Rajarathinam, A. M. Sadiq, and S. Rajeshkumar, "Anticancer activity of silver nanoparticles synthesized using aqueous fruit shell extract of *tamarindus* on MCF-7 human breast cancer cell line," *Journal of Drug Delivery Science and Technology*, vol. 55, Article ID 101376, 2020.

[20] A. H. Ahmed, M. Alsharidah, A. R. Osamah, M. T. Hesham, and N. S. Tolba, "Silver nanoparticle-coated ethyl cellulose inhibits tumer necrosis factor- α of breast cancer cells," *Drug Design, Development and Therapy*, vol. 15, pp. 2035–2046, 2021.

[21] L. Yang, C. Chen, Y. Hu et al., "Three-dimensional bacterial cellulose/polydopamine/TiO_2 nanocomposite membrane with enhanced adsorption and photocatalytic degradation for dyes under ultraviolet-visible irradiation," *Journal of Colloid and Interface Science*, vol. 562, pp. 21–28, 2020.

[22] J. Fan, D. Yu, W. Wang, and B. Liu, "The self-assembly and formation mechanism of regenerated cellulose films for photocatalytic degradation of C.I. Reactive Blue 19," *Cellulose*, vol. 26, no. 6, pp. 3955–3972, 2019.

[23] X. Wang, Y. Sui, J. Jian et al., "Ag@AgCl nanoparticles in-situ deposited cellulose acetate/silk fibroin composite film for photocatalytic and antibacterial applications," *Cellulose*, vol. 27, no. 13, pp. 7721–7737, 2020.

[24] K. Seku, S. S. Hussaini, B. Pejjai et al., "A rapid microwave-assisted synthesis of silver nanoparticles using Ziziphus jujuba Mill fruit extract and their catalytic and antimicrobial properties," *Chemical Papers*, vol. 75, no. 4, pp. 1341–1354, 2021.

[25] J. Wu, N. Zhao, X. Zhang, and J. Xu, "Cellulose/silver nanoparticles composite microspheres: eco-friendly synthesis and catalytic application," *Cellulose*, vol. 19, no. 4, pp. 1239–1249, 2012.

[26] J. Cai and L. Zhang, "Rapid dissolution of cellulose in LiOH/urea and NaOH/urea aqueous solutions," *Macromolecular Bioscience*, vol. 5, no. 6, pp. 539–548, 2005.

[27] S. Sathishkumar, C. Sridevi, R. Rajavel, and P. Karthikeyan, "Smart flower like MgO/Tb,Eu-substituted hydroxyapatite dual layer coating on 316L SS for enhanced corrosion resistance, antibacterial activity and osteocompatibility," *Journal of Science: Advanced Materials and Devices*, vol. 5, no. 4, pp. 545–553, 2020.

[28] Y. J. Xu, L. G. Zuo, X. Qian, and J. Wang, "Preparation and characterization of cellulose silver nanocomposites by in situ reduction with alkalis as activation reagent," *Bioresources*, vol. 11, no. 1, pp. 2797–2808, 2016.

[29] E. Smiechowicz, B. Niekraszewicz, P. Kulpinski, and K. Dzitko, "Antibacterial composite cellulose fibers modified with silver nanoparticles and nanosilica," *Cellulose*, vol. 25, no. 6, pp. 3499–3517, 2018.

[30] S. H. Barud, T. Regiani, F. C. Rodrigo, R. W. Marques, Y. Lustra, and J. L. R. Sidney, "Antimicrobial bacterial

cellulose silver nanoparticles composites membranes," *Journal of Nanomaterials*, vol. 2011, Article ID 721631, 8 pages, 2011.

[31] R. Jung, Y. Kim, H. S. Kim, and H. J. Jin, "Antimicrobial properties of hydrated cellulose membranes with silver nanoparticles," *Journal of Biomaterials Science, Polymer Edition*, vol. 20, no. 3, pp. 311–324, 2009.

[32] J. Wu, Y. Zheng, W. Song et al., "In situ synthesis of silver nanoparticles/bacterial cellulose composites for slow-released antimicrobial wound dressing," *Carbohydrate Polymers*, vol. 102, pp. 762–771, 2014.

[33] N. S. Alahmadi, J. W. Betts, T. Heinze, S. M. Kelly, A. Koschella, and J. D. Wadhawan, "Synthesis and antimicrobial effects of highly dispersed, cellulose-stabilized silver/cellulose nanocomposites," *RSC Advances*, vol. 8, no. 7, pp. 3646–3656, 2018.

[34] L. J. Del Valle, A. Diaz, and J. Puiggali, "Hydrogels for biomedical applications: cellulose, chitosan, and protein/peptide derivatives," *Gels*, vol. 3, p. 27, 2017.

[35] L. Kvitek, A. Panacek, J. Soukupová et al., "Effect of surfactants and polymers on stability and antibacterial activity of silver nanoparticles (NPs)," *Journal of Physical Chemistry C*, vol. 112, no. 15, pp. 5825–5834, 2008.

[36] L. Zhang, H. Lu, J. Chu et al., "Lignin-directed control of silver nanoparticles with tunable size in porous lignocellulose hydrogels and their application in catalytic reduction," *ACS Sustainable Chemistry & Engineering*, vol. 8, no. 33, Article ID 12655, 12663 pages, 2020.

[37] J. F. Moulder, W. F. Stickle, P. E. Sobol, and K. D. Bombem, "Handbook of X-ray Photoelectron Spectroscopy, Perkin-Elmer Corporation," *Eden Prairie, Minnesota*, vol. 38, p. 184, 1979.

[38] M. S. Islam, N. Akter, M. M. Rahman et al., "Mussel-inspired immobilization of silver nanoparticles toward antimicrobial cellulose paper," *ACS Sustainable Chemistry & Engineering*, vol. 6, no. 7, pp. 9178–9188, 2018.

[39] A. L. Gonzalez, C. Noguez, J. Beranek, and A. S. Barnard, "Size, shape, stability, and color of plasmonic silver nanoparticles," *Journal of Physical Chemistry C*, vol. 118, no. 17, pp. 9128–9136, 2014.

[40] R. Singaravelan and S. B. Sudarsan Alwar, "Electro chemical synthesis, characterization, phytogenic properties of silver nanoparticles," *Applied Nanoscience*, vol. 5, pp. 983–991, 2015.

[41] S. Dahle, J. Meuthen, W. Viol, and W. Maus-Friedrichs, "Adsorption of silver on cellobiose and cellulose studied with MIES, UPS, XPS and AFM," *Cellulose*, vol. 20, no. 5, pp. 2469–2480, 2013.

[42] S. Jain, G. Bhanjana, S. Heydarifard et al., "Enhanced antibacterial profile of nanoparticle impregnated cellulose foam filter paper for drinking water filtration," *Carbohydrate Polymers*, vol. 202, pp. 219–226, 2018.

[43] A. I. Nicoara, A. E. Stoica, D. I. Ene, B. S. Vasile, A. M. Holban, and I. A. Neacsu, "In situ and ex situ designed hydroxyapatite: bacterial cellulose materials with biomedical applications," *Materials*, vol. 13, no. 21, p. 4793, 2020.

[44] H. M. Ibrahim, "Green synthesis and characterization of silver nanoparticles using *banana peel* extract and their antimicrobial activity against representative microorganisms," *Journal of radiation research and applied sciences*, vol. 8, no. 3, pp. 265–275, 2015.

[45] P. Johnson, V. Krishnan, C. Loganathan et al., "Rabid biosynthesis of *bauhinia variegate* flower extract-mediated silver nanoparticles: an effective antioxidant scavenger and amylase inhibitor," *Artificial Cells, Nanomedicine, and Biotechnology*, vol. 46, no. 7, pp. 1488–1494, 2018.

[46] K. Venugopal, H. A. Rather, K. Rajagopal et al., "Synthesis of silver nanoparticles (Ag NPs) for anticancer activities (MCF7 breast and A549 lung cell lines) of the crude extract of *syzygium aromaticum*," *Journal of Photochemistry and Photobiology B: Biology*, vol. 167, pp. 282–289, 2017.

[47] M. Arumugam, B. Murugesan, N. Pandiyan, D. Kumar Chinnalagu, G. Rangasamy, and S. Mahalingam, "Electro-spinning cellulose acetate/silk fibroin/Au-Ag hybrid composite nanofibers for enhanced biocidal activity against MCF-7 breast cancer cell," *Materials Science and Engineering: C*, vol. 123, Article ID 112019, 2021.

[48] S. W. Chook, "Chin hua chia, chi hoong chan, siew xian chin, sarani zakaria, mohd shaiful sajab, and nay ming huang, "porous aerogel nanocomposite of silver nanoparticles-functionalized cellulose nanofibrils for SERS detection and catalytic degradation of rhodamine B," *RSC Advances*, vol. 1, no. 1, pp. 1–100, 2013.

[49] S. P. Vinay and N. Chandrasekhar, "Facile green chemistry synthesis of Ag nanoparticles using *areca catechu* extracts for the antimicrobial activity and photocatalytic degradation of methylene blue dye," *Materials Today: Proceedings*, vol. 9, pp. 499–505, 2019.

[50] I. Fatimah, I. Sahroni, O. Muraza, and R. Doong, "One-pot biosynthesis of SnO_2 dots mediated by *clitoria ternatea* flower extract for photocatalytic degradation of rhodamine B," *Journal of Environmental Chemical Engineering*, vol. 8, no. 4, Article ID 103879, 2020.

[51] P. Govindhan and C. Pragathiswaran, "Synthesis and characterization of $TiO_2@SiO_2$–Ag nanocomposites towards photocatalytic degradation of rhodamine B and methylene blue," *Journal of Materials Science: Materials in Electronics*, vol. 27, no. 8, pp. 8778–8785, 2016.

[52] J. Liu, Z. Shi, X. Li, J. Yang, and J. Lang, "ZnO nanorod arrays decorated with AgCl nanoparticles as highly efficient visible light driven photocatalyst," *Journal of Materials Science: Materials in Electronics*, vol. 30, no. 14, Article ID 13690, 13697 pages, 2019.

[53] Y. Kucukcobanoglu and M. Ayisigi, "Selin Haseki, and Lale Yildiz Aktas, "In situ green synthesis of cellulose based silver nanocomposite and its catalytic dye removal potential against methylene blue," *Journal of Cluster Science*, vol. 33, pp. 1623–1633, 2022.